PAPER

Check for updates

The impact of electrolytic pH on photoelectrochemical water oxidation†

Neeraj Kumar Biswas, [ID] [abc] Anupam Srivastav, [b] Sakshi Saxena, [bd] Anuradha Verma, [b] Runjhun Dutta, [ID] [b] Manju Srivastava, [b] Sumant Upadhyay, [e] Vibha Rani Satsangi, [ID] [f] Rohit Shrivastav [b] and Sahab Dass [ID] *[b]

Harnessing solar energy for clean and sustainable fuel production by photoelectrochemical water oxidation over different timescales has been extensively investigated. However, the light-driven photoelectrochemical water oxidation reaction for artificial photosynthesis suffers from poor photon-to-current efficiency. Herein, we demonstrate an experimental analysis of electrolytic pH on photoelectrochemical syngas production by varying the pH of the KOH and NaOH electrolytes using the N–ZnO photoelectrode and analyzing all variables. A maximum photocurrent of 13.80 mA cm^{-2} at 1.23 V *vs.* RHE with a 43.51% photon-to-current conversion efficiency was obtained at pH 13 in the aqueous NaOH electrolyte.

Introduction

The global demand for sustainable energy and related environmental crises have motivated scientists worldwide to find eco-friendly and renewable energy sources.[1,2] Photoelectrochemical water splitting, popularly known as artificial photosynthesis, produces green and sustainable fuel for environmental remediation.[3] The photoelectrochemical (PEC) system is an attractive way for solar energy conversion (*via* water splitting) toward generating green hydrogen fuel.[4] Water splitting is a thermodynamically difficult and kinetically sluggish reaction, which requires 1.23 V to evolve O$_2$ and H$_2$ molecules. Efforts have been made to improve the PEC performance of semiconductor materials (ZnO, α-Fe$_2$O$_3$, BiVO$_4$, and TiO$_2$) for hydrogen production like doping, heterojunctions, plasmons, *etc.*[5–11] However, as part of these modification strategies developed to improve PEC response for water splitting, the band edge position and charge carrier, solution conductivity, *etc.* are some of the issues that need more attention.

The band edge position at the semiconductor/electrolyte interface and the charge density of the electrolyte are the most fundamental properties that affect PEC performance. Zinc oxide (ZnO) is a non-toxic n-type semiconductor with an appropriate band edge position and stability and has emerged as one of the most promising PEC candidates.[12–22] ZnO occurs in the form of three crystal systems: wurtzite, zinc blend, and rock salt. The wurtzite crystal structure shows photocatalytic activity and thermodynamic stability and is easy to synthesize.[23] However, the band edge position of ZnO and the search for suitable electrolytes remain as obstacles to producing scalable efficiency in solar syngas production. Previous studies on ZnO-based PEC systems have focused on nanostructuring, metal or non-metal doping, heterojunctions, surface modification with plasmon modification, quantum dot modification, *etc.*[24–28] Nitrogen incorporation in ZnO reduces the optical band gap and improves absorption in the solar spectrum for better PEC efficiency.[29–37] However, the effect of pH on electrolytes and their effect on PEC activity have not been reported. Acidic electrolytes increase corrosion, while KOH and NaOH are basic electrolytes that provide a stable medium for metal oxides in PEC water splitting towards solar hydrogen production.[29]

The positions of the valence band energy (E_{vb}) and conduction band energy (E_{cb}) of N–ZnO straddle well with the water redox potential. In this study, we have attempted to explain the effect of pH of electrolytes on the band edge positions at the semiconductor/electrolyte interface using different electrolytes. In addition to this, the effect of NaOH and KOH in terms of the charge density of metal ions present in the electrolytes is also investigated.

Here, we demonstrate the pH effect on PEC water-splitting performance based on results obtained at different pH, *viz.* 9,

[a] Department for Continuing Education, University of Oxford, Rewley House, 1 Wellington Square, Oxford, OX1 2JA, UK. E-mail: sahabdas@dei.ac.in; drsahabdass@gmail.com

[b] Department of Chemistry, Faculty of Science, Dayalbagh Educational Institute Agra, 282005, India

[c] School of Foreign Languages, Aligarh Regional Centre, Indira Gandhi National Open University, Maidan Garhi, New Delhi – 110068, India

[d] Mangalayatan University, Beswan, Aligarh, Uttar Pradesh, India

[e] Amity University, Noida Campus, Sector 125, Noida, 201313, Uttar Pradesh, India

[f] Department of Physics, Faculty of Science, Dayalbagh Educational Institute Agra, 282005, India

10, 11, 12, 13, and 14 of the electrolytes (KOH and NaOH) using N–ZnO thin films. The study reveals that the band edge position is upshifted at the electrolyte/semiconductor interface with rising pH, reducing the photocurrent onset potential. In addition, the Na^+ ion in NaOH contains a higher charge density than the K^+ ion in KOH, which facilitates more polarization in water. This polarity profile in the PEC solvent induces binding energy, which improves charge transfer efficiency. PEC characterization in the present study confirms that the rise in electrolyte pH improves photoelectrochemical activity.

Experimental section

Structural characterization

The XRD patterns were recorded on a Bruker AXS D8 X-ray Diffractometer operated at 40 mA and 40 kV using a Cu Kα source. Field emission scanning electron microscopy (FESEM) was carried out using a JEOL JSM-7610F Plus Field Emission SEM. The diameter distributions of the particles in the samples were measured using Image J software. The atomic composition of the samples was analysed using energy dispersive X-ray (EDAX) analysis (Peltier cooled, Octane plus model (30 mm² and 127 eV resolution)). The Brunauer–Emmett–Teller (BET) surface area analysis was carried out using a BET Surface Area Analyzer Model/Supplier: Autosorb I; Quantachrome Corp. The photoluminescence (PL) lifetime was calculated using FLS920, Edinburgh Instruments, Scotland.

Preparation of the photoelectrode

The nanostructured N–ZnO photoelectrode was prepared according to a previously reported method.[38] Briefly, 1.5 g zinc acetate dihydrate $(Zn(CH_3COO)_2 \cdot 2H_2O$, 98% pure, Sigma-Aldrich) and 5 mL diethanolamine $(HN(CH_2CH_2OH)_2$, 98% pure, Merck) were added to 20 mL ethanol $(C_2H_5OH$, 97% pure, Sigma-Aldrich), and the solution was stirred for sol preparation. The precursor sol was spin-coated using a spin NXG-P2 instrument at 3000 rpm for 30 s on 1.1×1.1 cm⁻² pattern ITO glass (8–12 Ω sq⁻¹, SPI Supplies). The samples were sintered at 773 K for 2 hours to form nanostructured thin films. After the calcination process, N–ZnO/ITO was developed into a photoelectrode with an effective surface area of 1×1 cm⁻² connected by a copper wire and silver paste, and sealed with epoxy resin (Hysol, Singapore). The best photoresponse was observed for N–ZnO having a thickness of 327 nm. Further, the PEC system was fabricated using the N–ZnO thin films of 327 nm thickness.

Photoelectrochemical measurements

All PEC water splitting experiments were performed using a potentiostat (Zehner Zenium, Germany) in the three-electrode configuration between at −1 V and 1 V *vs.* RHE (20 mV s⁻¹ scan rate) in the potential range using of electrolytes (KOH and NaOH) at pH 9–14. The standard calomel electrode and platinum electrode were used as the counter and reference electrodes, respectively. The photoelectrode was irradiated with a 300 W xenon–mercury arc lamp (Newport Oriel) with a 139 mW cm⁻² power density. 1×1 cm⁻² was the area of the working electrode. The flat band potential (V_{fb}) was extracted from the slope using the following equation:

$$\frac{1}{C_{sc}^2} = \left(\frac{2}{e\varepsilon\varepsilon_o N_D}\right)\left(V_{app} - V_{fb} - \frac{k_b T}{e}\right) \quad (1)$$

where C_{sc} is the interfacial capacitance, e is the elementary charge, $\varepsilon = 8.5$ was used as the relative permittivity of N–ZnO, ε_o is the vacuum permittivity, N_D is the donor density, V_{fb} is the flat band potential, k_b is the Boltzmann constant, and T is the absolute temperature.[39]

N_D was analyzed using eqn (2):

$$S = \left(\frac{2}{e\varepsilon\varepsilon_o N_D}\right) \quad (2)$$

where S is the slope of the Mott–Schottky curve.[40]

The Fermi level was measured by using the following theoretical equation:

$$E_f = \frac{1}{2}(E_c + E_v) + kT \ln\left(\frac{m_p^*}{m_e^*}\right)^{\frac{3}{2}} + kT \ln \frac{N_D}{n_i} \quad (3)$$

E_f is the Fermi level, E_v is the energy of the valence band, E_c is the energy of the conduction band, m_e^* is the effective mass of the negative charge carriers (electron), m_p^* is the effective mass of the positive charge carriers (holes), T is the temperature, and n_i is the number of electrons per unit volume in an intrinsic semiconductor.

The conduction band (E_{cb}) was measured from the following theoretical equation:

$$n = 2\left(\frac{2\pi m_e^* kT}{h^2}\right)^{\frac{3}{2}} e^{-(E_{cb} - E_f)/kT} \quad (4)$$

where n is the concentration of free electrons in E_{cb}

The valence band (E_{vb}) was calculated from the following theoretical equation:

$$p = 2\left(\frac{2\pi m_h^* kT}{h^2}\right)^{\frac{3}{2}} e^{-(E_f - E_{vb})/kT} \quad (5)$$

where p is the concentration of free holes in E_{vb}.[41]

The External Quantum Efficiency (EQE) or incident photon-to-current conversion efficiency (IPCE) was calculated using the following equation:

$$EQE = \frac{1240 \times J_{ph}}{\lambda \times P} \quad (6)$$

where J_{ph} is the photocurrent density, P is the intensity of the incident light, and λ is the wavelength of the incident light.[42]

The fluorescence lifetime was calculated for nanostructured N–ZnO at an excitation wavelength of 490 nm using the following formula:

$$I(t) = \sum_{i=1}^{3} f_i \exp\left(-\frac{t}{\tau_i}\right) \quad (7)$$

where $I(t)$ is the fluorescence intensity at time t, τ_i is the fluorescence lifetime, and f_i is the amplitude when the sum of all f values is unity.

Results and discussion

The X-ray diffraction (XRD) pattern of N–ZnO showed three peaks for the (100), (002), and (101) planes (Fig. S1†), confirming that the as-grown thin film had the wurtzite phase (hexagonal system, JCPDS database file 36-1457). FESEM imaging of the photoelectrodes (Fig. S2†) confirmed successful photocatalyst deposition, with an average particle size of 47 nm (Fig. S3†). The chemical composition of the film based on EDAX confirmed the deposition of nanostructured N–ZnO on the ITO glass substrate (Fig. S4, and Table S1†). The photoluminescence (PL) lifetime was measured for nanostructured N–ZnO as 4.46 nm (Fig. S5†). The Brunauer–Emmett–Teller (BET) analysis of nanostructured N–ZnO was performed for the calculation of surface area (Fig. S6†), and a value of 1.853×10^{-4} m^2 g^{-1} was observed.

The photoelectrode made of nanostructured N–ZnO thin films with 327 nm thickness exhibited the maximum

photocurrent due to its better light-harvesting performance and improved charge transfer rate, and was selected for the investigation of the effect of varying pH on PEC performance in different electrolytes. The schematic view of this study is shown in Fig. 1. The PEC properties of the N–ZnO electrode were investigated at five different pH using two different electrolytes, *viz.* KOH and NaOH.

Solar-driven PEC water-splitting was studied at six different pH in two electrolytes *viz.* KOH and NaOH using nanostructured N–ZnO photoelectrode under 139 mW cm^{-2} illumination, as shown in Fig. 1. The maximum photocurrent density of 13.80 mA cm^{-2} was achieved at pH 13 in the NaOH electrolyte, and 11.30 mA cm^{-2} was obtained in the KOH electrolyte (see Fig. 2(a and b)). With a reduction in pH, *i.e.*, from pH 12 to 9, a decline in photocurrent density could be seen (Table 1). The molar ratio of the electrolytes increased with the rise in pH, as shown in Table S2,† and the literature shows that the viscosity of the aqueous NaOH solution is more than that of the KOH electrolytes (as shown in Fig. S7†).[43] We measured the photocurrent density in the range of 0.02–0.08 mA cm^{-2} at the lower pH values 9–11 in both the electrolytes due to the low concentration of electrolytes (*i.e.* 0.00001 M to 0.01 M). The values presented in Table 1 indicate that photocurrent density increased up to an optimum pH (pH 13) and then started decreasing, which may be attributed to the increasing photoexcited carrier recombination rate and slower ionic movement under illumination at higher pH.[44] The current density under dark conditions was approximately zero at different pH due to the insulating nature of N–ZnO in the dark (see Fig. 2(c and d)). The higher charge density of the Na$^+$ ions facilitates the higher polarization of hydronium and hydroxyl ions, thus improving the photoresponse in NaOH in comparison with KOH. This is responsible for the reduction in the overpotential requirement for water splitting to take place.[44,45]
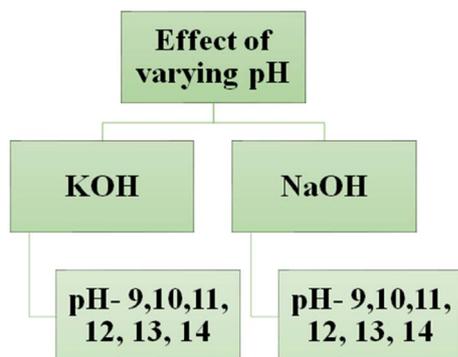

Fig. 1 The schematic view of the study of effect of varying pH on PEC performance in various electrolytes.
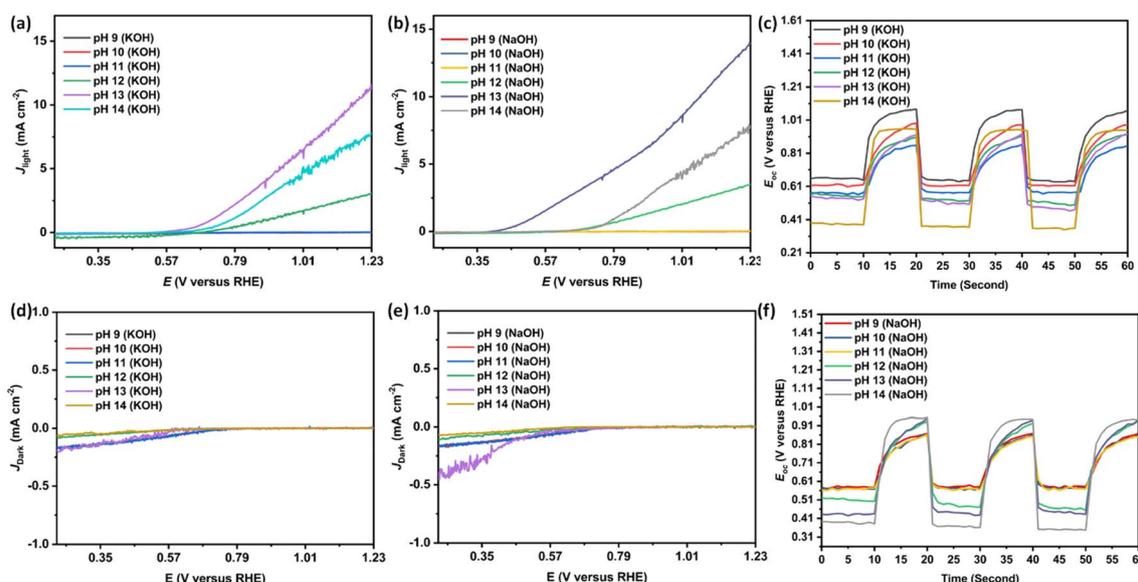

Fig. 2 (a and b) The photocurrent density of nanostructured N–ZnO at pH 9–14 in aqueous NaOH and KOH electrolytes. (c and f) The open-circuit voltage. (d and e) The dark current density of N–ZnO at pH 9–14 in aqueous NaOH and KOH electrolytes.

Table 1 Photocurrent density of 327 nm thick N–ZnO thin film electrode in aqueous NaOH and KOH electrolytes at different pH

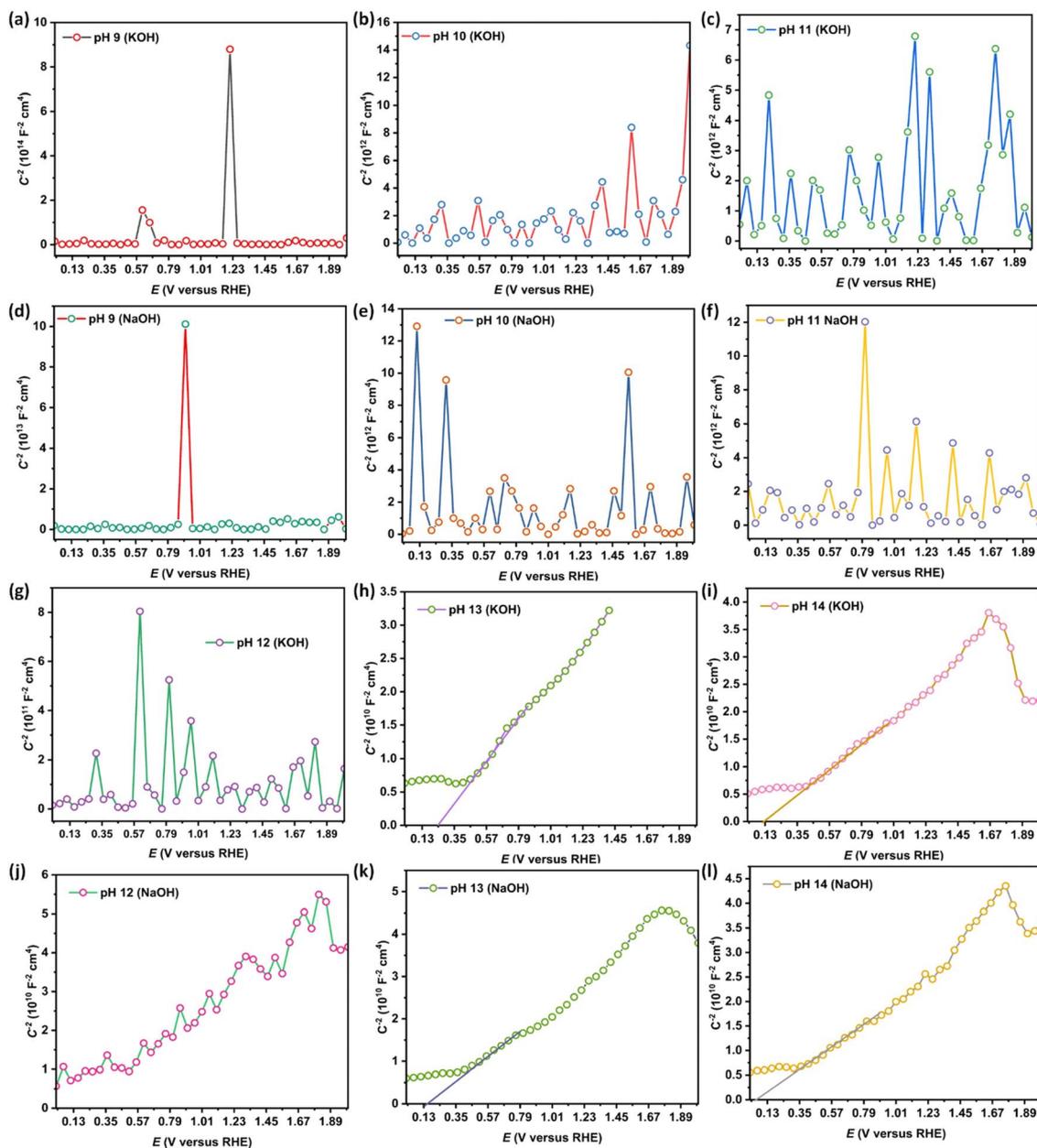|	Photocurrent density (mA cm^{-2})		Values of open-circuit voltage (V_{oc} vs. RHE)	
pH	KOH electrolyte	NaOH electrolyte	KOH electrolyte	NaOH electrolyte
9	0.02	0.04	0.62	0.58
10	0.05	0.06	0.61	0.57
11	0.06	0.08	0.57	0.55
12	1.24	3.51	0.49	0.45
13	**11.30**	**13.80**	0.46	0.42
14	7.60	7.50	**0.35**	**0.34**

Fig. 3 (a–l) The Mott–Schottky plots of nanostructured N–ZnO at pH 9–14 in the NaOH and KOH electrolytes.

Table 2 The flat band potential (V_{fb} vs. RHE) and donor density (cm^{-3}) of N–ZnO at different pH in aqueous NaOH and KOH electrolytes

| pH | Flat band potential (V_{fb} vs. RHE) | | Donor density (cm^{-3}) | |
	KOH electrolyte	NaOH electrolyte	KOH electrolyte	NaOH electrolyte
9	—	—	2.40×10^{16}	4.18×10^{16}
10	—	—	8.66×10^{16}	2.14×10^{17}
11	—	—	2.40×10^{17}	3.03×10^{17}
12	—	—	3.26×10^{17}	7.08×10^{18}
13	0.24	0.16	9.82×10^{18}	7.28×10^{18}
14	**0.12**	**0.05**	**1.07×10^{19}**	**8.24×10^{18}**

The decrease in open-circuit voltage (V_{oc} vs. RHE) was observed with an increase in pH, as shown in Fig. 2(c and f), which corroborate with the Mott–Schottky and EIS analyses. The least V_{oc} value in N–ZnO at higher pH confirms the decreased rate of photogenerated charge recombination. The values of V_{oc} vs. RHE measured for nanostructured N–ZnO at pH 9–14 in the KOH and NaOH electrolytes are given in Table 1.

Fig. 3(a–h) reveal noisy readings for nanostructured N–ZnO during the Mott–Schottky analysis on account of the low pH (9–12) of the KOH and NaOH electrolytes. The Mott–Schottky plot of the N–ZnO electrode exhibited a positive slope, characteristic of an n-type semiconductor. The flat band potential at pH 14 of NaOH was estimated as 0.05 V versus the reversible hydrogen electrode, which is lesser in comparison with the KOH electrolyte (as shown in Table 2 and Fig. 3(i–l)), confirming better charge separation at the semiconductor/NaOH electrolyte interface. From these analyses, it can be concluded that flat band potential depends on the pH of the electrolyte. An
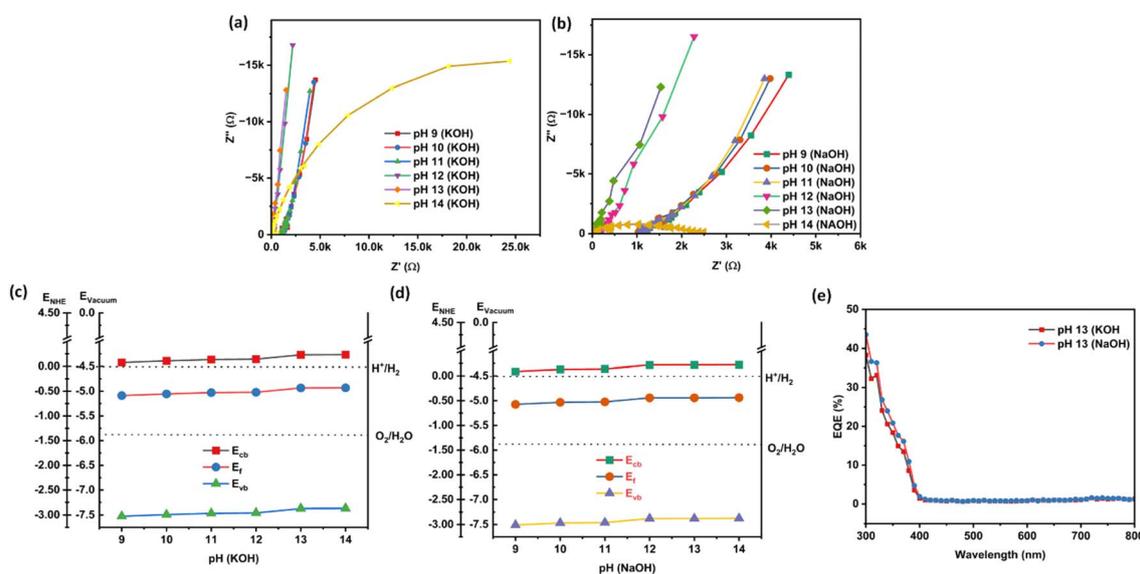

Fig. 4 (a and b) The Nyquist plots and (c and d) band edge positions of nanostructured N–ZnO pH at 9–14 in the NaOH and KOH electrolytes; (e) the external quantum efficiency (EQE) of nanostructured N–ZnO at pH 13 in aqueous (a) NaOH and (b) KOH electrolytes.

Table 3 The band edge positions of nanostructured N–ZnO at different pH in aqueous KOH electrolytes

| pH | Band edge position of nanostructured N–ZnO | | | | | |
| | KOH electrolyte | | | KOH electrolyte | | |
	E_{cb}	E_f	E_{vb}	E_{cb}	E_f	E_{vb}
9	−4.424 eV	−5.087 eV	−7.524 eV	−4.410 eV	−5.073 eV	−7.510 eV
10	−4.391 eV	−5.054 eV	−7.491 eV	−4.368 eV	−5.031 eV	−7.468 eV
11	−4.365 eV	−5.028 eV	−7.465 eV	−4.359 eV	−5.022 eV	−7.459 eV
12	−4.357 eV	−5.020 eV	−7.457 eV	−4.278 eV	−4.941 eV	−7.378 eV
13	−4.270 eV	−4.933 eV	−7.370 eV	−4.277 eV	−4.940 eV	−7.377 eV
14	−4.268 eV	−4.931 eV	−7.368 eV	−4.274 eV	−4.937 eV	−7.374 eV

increment in donor density was observed with rising pH in both KOH and NaOH electrolytes (as shown in Table 2).

Fig. 4(a and b) exhibit the charge transfer resistance properties of the N–ZnO photoelectrode at different pH values, as obtained by analyzing the Nyquist plots. At pH 14, a left shift in the semicircle was seen in both KOH and NaOH electrolytes, confirming the least solution resistance at the higher pH. Fig. 4(c and d) exhibit the band edge positions calculated using eqn (3)–(5). Table 3 shows the values of the band edge positions, *viz.* conduction band energy (E_{cb}), valency band energy (E_{vb}), and Fermi level energy (E_f).

It is visible from the findings that the downward shift of the conduction band is responsible for better charge separation at the semiconductor/electrolyte interface, which in turn corresponds with the better charge transfer rate. Fig. 4(e) presents the external quantum efficiency (EQE) values at pH 13 in the KOH and NaOH electrolytes. N–ZnO offers a 43.51% efficiency in the NaOH electrolyte and a 38.26% efficiency in KOH electrolyte.

Conclusions

In summary, nanostructured N–ZnO was deposited on the ITO glass substrate, and its PEC performance was studied using KOH and NaOH electrolytes in the pH range of 9–14. The maximum photoresponse was observed in the case of the NaOH electrolyte because Na^+ is more electropositive and has a high charge density than K^+, thus polarizing the water molecules more and lowering the energy requirement, as evident from the lower applied voltage required for water splitting in the NaOH electrolyte. To evidence the effect of electrolytic pH on water splitting, current–voltage, Mott–Schottky, EIS, V_{oc} measurements were carried out, which established the fact that higher pH values facilitate improvement in the water-splitting rate. Nanostructured N–ZnO exhibited low V_{fb}, high N_d, and V_{oc} value in the NaOH electrolytic conditions compared with the KOH electrolytes, and therefore, better efficiency was observed. The results also demonstrated that the band edge positions (E_{cb}, E_{vb} and E_f) of the semiconductor at the semiconductor/electrolyte interface upshifted with rising pH in both electrolytes. However, the photoresponse decreased with rising pH beyond the optimum pH of the electrolytes. These results show that the overall photocatalytic performance is regulated by various factors, and the more dominating factor decides the efficiency, as evidenced by the slowed ionic mobility and boosted conductivity at high pH.

Author contributions

Neeraj Kumar Biswas: conception, methodology, data curation, formal analysis investigation of data, writing-original drafting; Runjhun Dutta: data curation, formal analysis investigation of data; Anupam Srivastav: formal analysis and investigation; Sakshi Saxena: validation and resources; Anuradha Verma: writing-review and editing, validation, visualization; Manju Srivastava: validation and resources; Sumant Upadhyay: data curation, formal analysis investigation of data; Vibha Rani Satsangi: conceptualization, visualization; Rohit Shrivastav: conceptualization, visualization; Sahab Dass: writing-review and editing, visualization, supervision, project administration, funding acquisition.

Conflicts of interest

There are no conflicts to declare.

References

1 Y. Xiao, C. Feng, J. Fu, F. Wang, C. Li, V. F. Kunzelmann, C. M. Jiang, M. Nakabayashi, N. Shibata, I. D. Sharp and K. Domen, *Nat. Catal.*, 2020, **3**(11), 932–940.
2 X. Song, G. Wei, J. Sun, C. Peng, J. Yin, X. Zhang, Y. Jiang and H. Fei, *Nat. Catal.*, 2020, **3**(12), 1027–1033.
3 M. Grätzel, *nature*, 2001, **414**(6861), 338–344.
4 D. Gust, T. A. Moore and A. L. Moore, *Acc. Chem. Res.*, 2009, **42**(12), 1890–1898.
5 L. Liccardo, E. Lushaj, L. Dal Compare, E. Moretti and A. Vomiero, *Small Sci.*, 2021, **2**, 2100104.
6 A. J. Rettie, H. C. Lee, L. G. Marshall, J. F. Lin, C. Capan, J. Lindemuth, J. S. McCloy, J. Zhou, A. J. Bard and C. B. Mullins, *J. Am. Chem. Soc.*, 2013, **135**(30), 11389–11396.
7 E. Thimsen, F. Le Formal, M. Gratzel and S. C. Warren, *Nano Lett.*, 2011, **11**(1), 35–43.
8 A. M. Huerta-Flores, G. Chávez-Angulo, O. A. Carrasco-Jaim, L. M. Torres-Martínez and M. A. Garza-Navarro, *J. Photochem. Photobiol., A*, 2021, **410**, 113077.
9 M. Wang, F. Ren, J. Zhou, G. Cai, L. Cai, Y. Hu, D. Wang, Y. Liu, L. Guo and S. Shen, *Sci. Rep.*, 2015, **5**(1), 1–13.
10 R. Bengas, H. Lahmar, K. M. Redha, L. Mentar, A. Azizi, G. Schmerber and A. Dinia, *RSC Adv.*, 2019, **9**(50), 29056–29069.
11 N. K. Biswas, A. Srivastav, S. Saxena, A. Verma, R. Dutta, M. Srivastava, S. Upadhyay, V. R. Satsangi, R. Shrivastav and S. Dass, *Int. J. Hydrogen Energy*, 2022, **47**(53), 22415–22429.
12 N. Mufti, M. T. H. Abadi, A. Yasrina, M. Diantoro and A. Fuad, *IOP Conf. Ser.: Mater. Sci. Eng.*, 2019, **515**(1), 012023.
13 S. Arya, P. Mahajan, S. Mahajan, A. Khosla, R. Datt, V. Gupta, S. J. Young and S. K. Oruganti, *ECS J. Solid State Sci. Technol.*, 2021, **10**(2), 023002.

14 C. Vidya, C. Manjunatha, M. N. Chandraprabha, M. Rajshekar and A. R. MAL, *J. Environ. Chem. Eng.*, 2017, **5**(4), 3172–3180.

15 M. Jena, C. Manjunatha, B. W. Shivaraj, G. Nagaraju, S. Ashoka and M. S. Aan, *Mater. Today Chem.*, 2019, **12**, 187–199.

16 C. Manjunatha, B. Abhishek, B. W. Shivaraj, S. Ashoka, M. Shashank and G. Nagaraju, *Chem. Pap.*, 2020, **74**(8), 2719–2731.

17 C. Vidya, C. Manjunatha, M. Sudeep, S. Ashoka and L. A. Raj, *SN Appl. Sci.*, 2020, **2**(4), 1–15.

18 S. Banerjee, S. Padhan and R. Thangavel, *Mater. Chem. Phys.*, 2022, **277**, 125548.

19 S. S. Shinde, C. H. Bhosale and K. Y. Rajpure, *J. Photochem. Photobiol., B*, 2012, **113**, 70–77.

20 S. Goktas and A. Goktas, *J. Alloys Compd.*, 2021, **863**, 158734.

21 A. Goktas, I. H. Mutlu, Y. Yamada and E. Celik, *J. Alloys Compd.*, 2013, **553**, 259–266.

22 H. Nian, S. H. Hahn, K. K. Koo, E. W. Shin and E. J. Kim, *Mater. Lett.*, 2009, **63**(26), 2246–2248.

23 J. Kegel, I. M. Povey and M. E. Pemble, *Nano energy*, 2018, **54**, 409–428.

24 M. A. Desai, A. N. Vyas, G. D. Saratale and S. D. Sartale, *Int. J. Hydrogen Energy*, 2019, **44**(4), 2091–2127.

25 M. Ma, Y. Huang, J. Liu, K. Liu, Z. Wang, C. Zhao, S. Qu and Z. Wang, *J. Semicond.*, 2020, **41**(9), 091702.

26 Y. Li and J. Z. Zhang, *Laser Photonics Rev.*, 2010, **4**(4), 517–528.

27 R. B. Wei, P. Y. Kuang, H. Cheng, Y. B. Chen, J. Y. Long, M. Y. Zhang and Z. Q. Liu, *ACS Sustainable Chem. Eng.*, 2017, **5**(5), 4249–4257.

28 Y. Cai, C. Yao and J. Yuan, *J. Nanomater.*, 2020, **2020**, 6742728.

29 A. Sharma, M. Chakraborty and R. Thangavel, *J. Mater. Sci.: Mater. Electron.*, 2018, **29**(17), 14710–14722.

30 K. Jindal, M. Tomar, R. S. Katiyar and V. Gupta, *J. Appl. Phys.*, 2012, **111**(10), 102805.

31 F. Mikailzade, H. Türkan, F. Önal, Ö. Karataş, S. Kazan, M. Zarbali, A. Göktaş and A. Tumbul, *Appl. Phys. A: Mater. Sci. Process.*, 2020, **126**(10), 768.

32 H. Hopoğlu, H. S. Aydınoğlu, A. Özer and E. Ş. Tüzemen, *Opt. Mater.*, 2021, **122**, 111685.

33 A. Goktas, E. Aslan, F. Arslan and A. Kilic, *Opt. Mater.*, 2022, **133**, 112984.

34 A. Mekki, N. Tabet and M. Hezam, *Int. J. Nano Biomater.*, 2009, **2**, 216–225.

35 H. Gencer, M. Gunes, A. Goktas, Y. Babur, H. I. Mutlu and S. Atalay, *J. Alloys Compd.*, 2008, **465**(1–2), 20–23.

36 E. S. Rajalekshmi, V. A. Ferby, R. Shabu and A. M. E. Raj, preprint (version 1) available at Research Square, v12021.

37 A. Tumbul, A. Göktaş, M. Z. Zarbali and F. Aslan, *Mater. Res. Express*, 2018, **5**(6), 066408.

38 N. K. Biswas, A. Srivastav, S. Saxena, A. Verma, A. Banerjee, K. Asha, V. R. Satsangi, R. Shrivastav and S. Dass, Indian Patent 390045, 2022.

39 J. Cen, Q. Wu, M. Liu and A. Orlov, *Green Energy Environ.*, 2017, **2**(2), 100–111.

40 N. Singh, B. Kumari, S. Sharma, S. Chaudhary, S. Upadhyay, V. R. Satsangi, S. Dass and R. Shrivastav, *Renewable energy*, 2014, **69**, 242–252.

41 R. Van de Krol, Photoelectrochemical Hydrogen Production. Electronic Materials: Science & Technology, *Principles of photoelectrochemical cells*, ed. R. van de Krol and M. Grätzel, Springer, Boston, MA, 2011, vol. 102.

42 N. Murakami and K. Okuzono, *Chem. Commun.*, 2020, **56**(40), 5417–5420.

43 P. M. Sipos, G. Hefter and P. M. May, *J. Chem. Eng. Data*, 2000, **45**(4), 613–617.

44 N. K. Biswas, A. Srivastav, S. Saxena, A. Verma, R. Dutta, M. Srivastava, V. R. Satsangi, R. Shrivastav and S. Dass, *Sol. Energy*, 2022, **247**, 543–552.

45 N. K. Biswas, R. Dutta, A. Srivastav, S. Saxena, A. Verma, M. Srivastava, S. Upadhyay, V. R. Satsangi, R. Shrivastav and S. Dass, *Results Chem.*, 2022, **4**, 100675.